The Role of Repulsion in Colloidal Crystal Engineering with DNA

Soyoung E. Seo,^{†,‡} Tao Li,^{‡,‡} Andrew J. Senesi,[‡] Chad A. Mirkin,*,[†] and Byeongdu Lee*,[‡]

[†]Department of Chemistry and International Institute for Nanotechnology, Northwestern University, 2145 Sheridan Road, Evanston, Illinois 60208, United States

[‡]X-ray Science Division, Argonne National Laboratory, 9700 Cass Avenue, Lemont, Illinois 60439, United States

ABSTRACT: Hybridization interactions between DNA-functionalized nanoparticles (DNA-NPs) can be used to program the crystallization behavior of superlattices, yielding access to complex three-dimensional structures with more than 30 different lattice symmetries. The first superlattice structures using DNA-NPs as building blocks were identified almost two decades ago, yet the role of repulsive interactions in guiding structure formation is still largely unexplored. Here, a comprehensive approach is taken to study the role of repulsion in the assembly behavior of DNA-NPs, enabling the calculation of interparticle interaction potentials based on experimental results. In this work, we used two different means to assemble DNA-NPs—Watson-Crick base pairing interactions and depletion interactions—and systematically varied the salt concentration to study the effective interactions in DNA-NP superlattices. A comparison between the two systems allows us to decouple the repulsive forces from the attractive hybridization interactions that are sensitive to the ionic environment. We find that the gap distance between adjacent DNA-NPs follows a simple power law dependence on solution ionic strength regardless of the type of attractive forces present. This result suggests that the observed trend is driven by repulsive interactions. To better understand such behavior, we propose a mean-field model that provides a mathematical description for the observed trend. This model shows that the trend is due to the variation in the effective cross-sectional diameter of DNA duplex and the thickness of DNA shell.

Introduction

In nature, the structure of atomic crystalline solids is dictated by the inherent, electronic properties of the constituent atomic building blocks. Consequently, significant effort has been expended to understand these properties and develop rules that allow one to understand the thermodynamically favored crystal structures but with limited success. For example, Pauling's rules for ionic solids allow one to understand crystallization behavior, but they do not allow one to deliberately design crystal architecture since the possibilities are inextricably coupled to the identities of the elemental building blocks (cations and anions).1-3 Similarly, for nanoscale systems, the structures of colloidal crystals are dictated by the type of bonding interactions induced by various surface ligands, but unlike atoms, their bonding behavior can be decoupled from the compositional identity of the particle.4-8 For example, we have shown that DNA-NPs can be likened to programmable atom equivalents (PAEs) with bonding characteristics that correlate with the oligonucleotide sequence.4-7 When compared to atomic systems, the crystallization behavior of PAEs is analogous to that of ionic crystals, where DNA hybridization interactions can induce particle attraction similar to charge attraction between cations and anions in ionic crystals. Over a large design space, one can use the general principle that the structure which maximizes hybridization (attractive) interactions will be the most thermodynamically favorable structure.^{5, 9} This is known as the complementary contact model (CCM) and has been used to deliberately make over

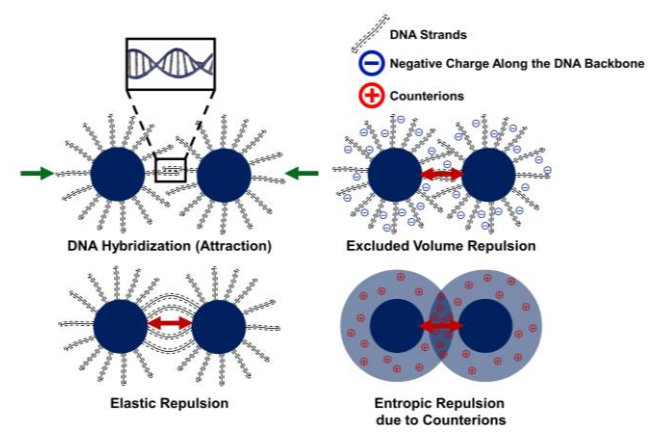
500 different crystals spanning over 30 different symmetries.5, 10-13

Although the general principle has been a reliable guide to design the vast majority of crystal structures explored with PAEs,5 it has been realized that the formation of certain structures cannot be explained solely through hybridization interactions. 14-16 Several observations have led to speculation that repulsion may also play a role in the crystallization behavior of PAEs.5, 14-15, 17-18 For example, the CsCl lattices have been observed in some cases when the CCM predicted AlB₂ symmetry; repulsion may account for the lower packing density between the two lattices.⁵ Furthermore, unlike atomic crystals, AlB₂ lattices synthesized from PAEs have lower c/a ratios than expected from DNA hybridization interactions alone $\sqrt{(8/3)}$, which may stem from repulsion between like-particles with non-complementary DNA strands, analogous to like-charge repulsion in ionic crystals. Last, in the case of anisotropic particles, the lamellar structures assembled with two-dimensional nanoparticles exhibit greater gap distance than the superlattices synthesized with spherical nanoparticles. This may occur because the denser negatively charged DNA shell on the flat face of the two-dimensional nanoparticles could exert a greater repulsive force between adjacent particles.¹⁷ Based on these observations, we hypothesize that the tendency of PAEs to transform to apparently lower symmetry/packing structure is a consequence of the system's tendency to minimize the repulsion between particles.

The origin of repulsion for the PAE system can be understood by studying the mechanical and chemical properties of DNA. Recently, Thaner et al.15 reported that the conformational entropies of flexible DNA strands can shift the crystallization pathway to favor the formation of lower packing structures (e.g. body-centered cubic, bcc) over the formation of high packing structures (e.g. face-centered cubic, fcc), which is a phenomenon often observed in diblock copolymer systems.¹⁹ To gain a theoretical understanding of the dominating forces that drive the assembly of PAEs, the interactions between DNA shells can be modeled by investigating the contributions of both attractive and repulsive energies to the overall lattice energy. While DNA base-pairing is the main attractive force driving the assembly, there are various types of repulsive interactions between DNA strands that prevent particles from coming closer than its contour (outstretched) length (Scheme 1). Briefly, one must consider the thermodynamic penalties involved in conformation stresses imposed on DNA chains that are participating in interactions between adjacent particles upon assembly.20-22 Furthermore, because DNA is a polyelectrolyte, the charge repulsion from the negatively charged DNA shell and the excluded volume repulsion should be considered, 23-24 along with the build-up of osmotic pressure due to counterions trapped in the DNA shell upon PAE assembly.25-26

Herein, we use the gap distance, a structural parameter of superlattices, as a means to measure the relative strength of attractive and repulsive forces. The change in interparticle gap distance as a function of varying ionic strength is probed, and then compared to the pair potential of the PAE superlattice, which was calculated using a mean-field theory based on classical polyelectrolyte brush theory combined with the mechanical properties of DNA.20, 23, 26 We first demonstrate that there is a power law relationship between the gap distance and the solution ionic strength. Further, we show that the excluded volume repulsion is the dominating repulsion in PAE assembly, and the variation in the effective diameter of DNA duplex and the thickness of the DNA shell are factors responsible for ionic strength dependent repulsion between PAEs. Although not directly addressed in this work, the DNA surface density can serve as a handle to tune the interparticle interactions similar to polyelectrolyte systems.²³ This pair potential calculation successfully reproduces the observed power law behavior (*Gap Distance* = $a + b \cdot (Salt Concentration)^{-0.5}$) and can be used to predict the lattice stability in a system that was previously not understood.5 Our mathematical description of the interaction potential energies not only provides the opportunity to precisely modulate the design parameters related to the individual PAE building blocks but also has the potential to allow one to deliberately design structures with lower packing density and importantly, create models for targeting structures prior to assembly.27-29

Scheme 1. A schematic representation of various interactions between DNA-modified nanoparticles.



Results

Assembly of Colloidal PAEs Through DNA Hybridization Interactions

We used a four-stranded DNA system to link adjacent particles through hybridization events. Each particle contained a DNA strand tethered to the nanoparticle's surface consisting of a thiol-modified "spacer" segment (a hexaethylene glycol phosphate oligomer) and an 18-base duplexer region. The second strand, the DNA linker, consists of a complementary 18-base duplexer region, a flexor segment (a hexaethylene glycol phosphate oligomer), and a 7base recognition region, also known as a "sticky end" (Table S₁). We prepared two types of particles with A-type and B-type sticky end linkers, whose sequences are complementary. The PAEs with non-complementary sticky ends will not interact with each other since the hybridization interaction between the sticky ends is the main attractive force that drives the assembly. The PAEs were assembled by mixing the DNA-functionalized particles hybridized with corresponding linkers and then allowed to aggregate. The aggregates were subsequently annealed a few degrees below the melting temperature to transform the disordered structure into the ordered superlattice. The sticky end sequences and the particle sizes used for this study allow the PAEs to reorganize into a bcc structure (Figure S1).5 Synthesized crystals were analyzed in solution with synchrotron-based small angle X-ray scattering (SAXS), where the lattice parameter can be determined by indexing the scattering peaks,30 and was subsequently used to calculate the surface-to-surface distance or the gap distance, D, between two nearest neighbor PAEs.

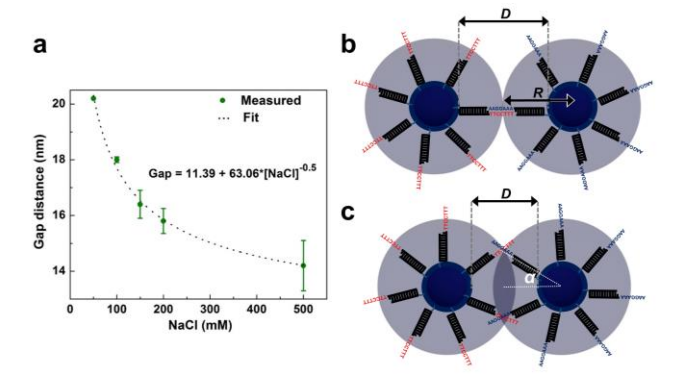


Figure 1. a) SAXS characterization shows that the gap distance for a bcc structure formed via hybridization interactions decreases with increasing salt concentration. The dotted line represents the power law fit. b) The maximum gap distance can be achieved when two nearest neighbor PAEs are in contact with each other, which is typically observed at lower salt concentration. c) A decrease in gap distance results in more overlap between the complementary DNA shells of adjacent PAEs. The overlap becomes more significant as the salt concentration is increased. The overlapping region of the DNA shells is highlighted as dark blue. The variable α is discussed in the SI.

The effect of salt concentration on PAE superlattices was studied by measuring the change in *D* at different salt concentrations. We find that *D* decays exponentially with increasing salt concentration according to an empirical power law [I]-0.5 (Figure 1a), where [I] is the NaCl concentration in mM. An extrapolated formula for the observed decaying trend in Figure 1a can be given by the following expression:

$$D = L_s + L_c \cdot [I]^{-0.5}$$
 Eq. 1

 L_S is the steric term which is not dependent on the ionic strength and is equal to the smallest gap distance that can be achieved. The second term L_C depends on salt concentration and is thus related to the electrostatic contribution from the negatively charged DNA phosphate backbones. Over a substantial range, as the salt concentration increases, the gap distance decreases, which indicates that there is an increased overlap between DNA shells of adjacent PAEs. Therefore, under the assumption that the thermodynamic penalty of altering DNA conformation is relatively small, a greater number of sticky ends can hybridize, leading to the formation of a more stable structure.

The maximum bond length that can be achieved with our PAE design can be determined. In principle, since the PAE assembly initiates upon contact between complementary sticky ends, an upper bound limit for the theoretically achievable gap distance is approximately twice the DNA shell thickness, L_o (Figure 1b). L_o is equivalent to the sum of the lengths of the different segments on DNA strands that connect two particles (Eq. S2). The conformation of the duplexed DNA tethered to the surface is assumed to be similar to that of canonical B-form DNA at 500 mM NaCl, which has a rise per base pair, l_b , of 0.34 nm.³¹ Thus, based on L_0 , the maximum D is 19.4 nm (Eq. S2). However, this value is smaller than the gap distance of the PAE lattices assembled at 50 mM NaCl because the length of the spacer and flexor segments used for this calculation was measured at 500 mM NaCl (Figure 1a).32 Since the single-stranded spacer and flexor segments are negatively charged, the flexibility of these segments allows them to be in a more stretched-out conformation at lower salt concentration due to phosphate-to-phosphate repulsion.33-34 Furthermore, while it has been shown that the persistence length of DNA does not change significantly with ionic strength, 20,

 35 the elastic modulus decreases at lower salt concentration, making DNA susceptible to elongation. 20 Therefore, the length used to calculate the gap distance at low salt condition is underestimated. Later in the analysis, the theoretical gap distances for both fixed and variable L_o values with changing salt concentration were calculated and compared with the experimental results.

To evaluate the strength of attractive force from hybridization interactions, a simple expression for the attractive interaction potential between PAEs was derived in Eq. 2 based on the CCM.⁵

$$\frac{E_{Attractive}}{kT} = -\sigma f_s e_h$$
 Eq. 2

where σ is the total number of the sticky ends on the particle, e_h is the hybridization energy of each sticky end, and *E*_{Attractive} is the attractive interaction potential. The CCM assumes that the strength of attractive force is proportional to the fractional surface area that overlaps between adjacent particles, a spherical cap (Figure 1c). The areal fraction of the overlap can be simplified as $f_s = (R - d/2)/(2R)$, where *R* is the radius of the PAE and *d* is the interparticle distance (center-to-center distance) (Eqs. S6-S13, see the full derivation for both identical and non-identical particles in the Supporting Information, SI). Assuming that the persistence length of the DNA duplex does not vary dramatically within the range of monovalent salt concentrations probed,^{20, 35} for example, approximately 5% of the total surface area of a DNA shell is occupied between two interacting PAEs, thus 40% of the total surface area between its eight neighbor PAEs in a bcc structure based on the experimentally determined D at 500 mM NaCl (Figure S2). As D becomes smaller, E_{Attractive} becomes more negative with an increase in f_s . Therefore, the crystals are expected to be more stable at higher salt concentration. Based on Eq. 2, E_{Attractive} is approximately -1,700 kT at 500 mM NaCl. It is important to note that this value is based on the strength of individually weak DNA binding events. Because PAEs exhibit highly cooperative binding properties,³⁶⁻³⁷ the attractive force that holds the particles together as a whole should be greater. Furthermore, e_h increases with salt concentration as a stronger charge neutralization of the DNA backbone consequently makes the DNA binding more favorable.³⁸⁻³⁹ Therefore, because the addition of salt alters both the attractive and repulsive forces, this presents an experimental limitation in decoupling the free energy contributions from various interactions using this system.

Assembly of Colloidal PAEs Through Depletion Forces

To decouple the salt-dependent contributions of attraction and repulsion, we assembled non-complementary PAEs in the absence of the possibility of hybridization interactions (i.e. the sticky end sequences do not interact through basepairing) using depletion forces as a driver for particle assembly. Upon addition of the polymer depletant (carboxymethylcelluose (CMC)), the polymer phase separates from the PAE aggregates to maximize the space that the

polymer can occupy, which creates an overlap between the exclusion layers of PAEs thereby resulting in superlattice formation (Figure 2a).40-43 The depletion force can be considered as an osmotic pressure since the polymer depletants will exert pressure to the particles due to a local polymer concentration gradient created between the exclusion volume and the solution. Our calculation indicates that while the osmotic pressure is weaker at higher salt concentrations, it does not vary significantly over the range of salt concentrations probed in this study, which allows us to use *D* as a direct measure of the strength of the repulsion since the attractive force remains constant (Figure S₃). At 50 mM NaCl, the PAEs assembled into fcc lattices upon addition of the CMC. At higher salt concentrations, they formed a mixture of fcc and amorphous structures (Figure S4). Because the steric and charge distributions of the DNA shell will be different at varying salt concentrations in the presence of different number of linkers, we added the maximum number of linker equivalents (600 and 900 linker equivalents) to ensure that the observed trend does not result from varying linker loading (Figure S5, see the discussion in the SI).

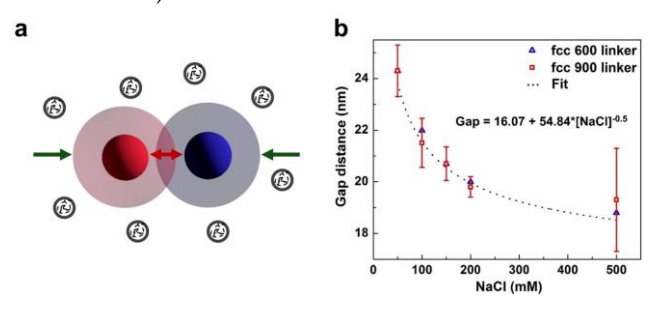


Figure 2. a) A schematic representation of the PAE superlattice formation using depletion forces. Small grey spheres represent the depletants. b) Gap distances plotted as a function of salt concentration for the superlattices assembled through depletion forces.

Remarkably, we observed that these structures display a similar exponentially decaying trend with the same exponent of -0.5 as typical PAE superlattices (Figure 2b). This result reveals that the repulsion is responsible for the observed power law behavior since the applied osmotic pressure that brings particles together is constant at the range of salt concentrations probed for this system (Figure S₃). However, there is a distinction between hybridization and depletant based systems in that the gap distances of lattices formed via depletants are consistently greater than those formed via hybridization interactions between short sticky ends. Because the sticky ends do not hybridize for the depletion based system, there are more DNA bases between adjacent PAEs, resulting in a larger interparticle distance. This discrepancy in the gap distances between two systems can be shown by comparing the attractive potential energies of the depletion and the hybridization based systems; the magnitude of attractive force induced for the depletion system⁴⁰ (-430 kT) is smaller than that of the hybridization system (-1,700 kT).

Discussion

The Role of Repulsion in PAE Assembly

We used a mean-field theory to understand the repulsive interactions between PAEs and calculate the pair potential of the PAE superlattice by calculating the change in free energy before and after assembly, which successfully reproduces the experimentally observed empirical formula (Eq. 1). To construct a theoretical model that can rationally explain PAE assembly behavior, we assume that the DNA duplexes grafted on the nanoparticle's surface behave like semi-flexible polyelectrolyte brushes.

The free energy calculation of grafted polyelectrolyte brushes consists of three major components: the steric (polymeric) and electrostatic contributions of the polyelectrolytes, and the entropic contribution of the counterions and coions (supporting electrolyte).26,44 Despite the large amount of negative charge surrounding the PAEs, the range in which the electrostatic repulsion has an influence does not extend farther than the thickness of the brush layer (DNA shell thickness).44-45 Additionally, the longrange electrostatic repulsion between particles should be effectively screened by counterions and salt ions for the range of salt concentrations probed in this study.^{5, 45-48} Therefore, we neglected the long-range Coulombic repulsion between PAEs in our derivation, but we implemented the electrostatic repulsion between DNA chains by integrating the Debye length into the effective radius of the DNA duplex, R_{DNA} (Figure 3). We mainly considered the short-range repulsive interactions between DNA chains such as excluded volume repulsion in the overlap (Figure 3), elastic repulsion from DNA chains connecting two particles (Figure 4), and repulsion from entropic effects due to counterions within the DNA shell overlap (Scheme 1).

Excluded Volume Repulsion

Simply, the excluded volume repulsion refers to the idea that a space occupied by a chain molecule cannot be occupied by another polymer chain. In polymer science, this concept mainly takes into account short-range features such as structural geometry and steric interactions between neighboring polymer chains. By adopting the grafted polymer brush theory,23 the excluded volume repulsive potential can be calculated as ΠV_o , where Π is the osmotic pressure is from the pressure difference between the overlap and the solution, and V_0 is the total volume of the overlap. According to the mean-field model of the concentrated polymer brushes, 23, 49 the osmotic pressure is defined as $vc^2/2$, where v is the excluded volume of a monomer and *c* is the monomer concentration within the overlap volume. The term vc represents the volume fraction of DNA chains in the overlap, which varies as a function of radial distance. Therefore, $vc = V_{DNA}/V_o$, where V_{DNA} is the volume occupied by DNA chains within the overlap and V_o is $(\pi/12)(4R+d)(2R-d)^2$.

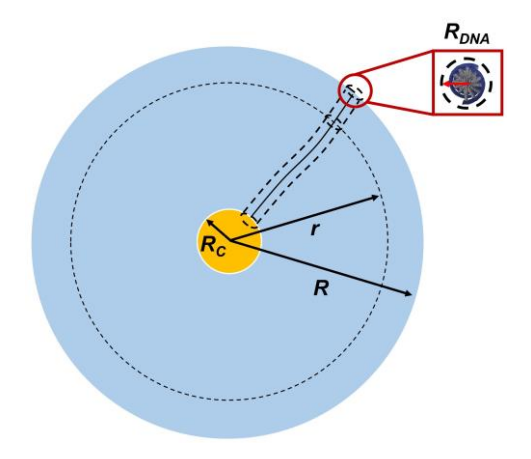


Figure 3. A model of a PAE where the DNA duplex is depicted as a simplified semi-flexible cylinder with a radius of R_{DNA} .

To quantify the volume fraction occupied by DNA chains in the overlap, we first simplified each DNA strand as a semi-flexible rod-like chain (Figure 3). Then, we defined the area fraction occupied by DNA chains at a distance r from the center of a PAE as (Figure 3):

$$\begin{split} &\rho_{DNA}(r) \\ &= \frac{SA\ of\ DNA\ duplexes\ at\ r}{SA\ of\ a\ PAE\ at\ r} \\ &= \frac{\sigma\pi R_{DNA}^2}{4\pi r^2} \end{split}$$
 Eq. 3

where SA stands for the surface area. R_{DNA} is a measure of the bulkiness of DNA chain along the radial direction (Figure 3). R_{DNA} changes as a function of salt concentration, and it can be expressed as:

$$R_{DNA} = R_0 + \kappa^{-1}$$
 Eq. 4

where R_o is the radius of DNA duplex (1 nm for B-form DNA)⁵⁰⁻⁵¹ and κ^{-1} is the Debye length, which depends on solution ionic strength (Eqs. S4 and S5). Note that κ^{-1} decreases with increasing ionic strength due to charge screening. Therefore, the effective cross-sectional area, πR_{DNA}^{-2} , of a single DNA chain is greater at lower salt concentration, and thus the volume that a DNA chain can occupy is larger. Then, the total volume of the DNA duplexes within the overlap can be calculated as:

$$V_{DNA}(d, R) = 2 \int_{d-R}^{R} \rho_{DNA}(r) dr$$
 Eq. 5

By integrating $\rho_{DNA}(r)$, the volume occupied by DNA duplexes within the overlap can be derived as:

$$V_{DNA} = \sigma \pi R_{DNA}^2 \psi(d, R)$$
 Eq. 6

The detailed mathematical formula for $\psi(d,R)$ is provided in the SI. An increase in V_{DNA} will result in increased steric

repulsion. A simplification of full derivation reveals that the terms that vary with ionic strength is R_{DNA} and R (Eqs. S14-S22). By incorporating $R = R_C + L_o$, we were able to define R as a function of varying L_o with changing salt concentration.

By defining one base pair to be a monomeric unit and a volume of a monomer to be $v = \pi R_{DNA}^2 l_b$, we can solve the excluded volume repulsion potential as:

$$\frac{E_{Excluded\ Volume}}{kT} = \sigma^2 \pi R_{DNA}^2 \frac{\psi(d,R)^2}{l_b V_0}$$
 Eq. 7

This equation can be generalized to a set of two different sized PAEs (Eqs. S23-S28). We note that this potential energy can also be calculated using Flory-Krigbaum theory for mixing of dilute polymer solutions⁵²⁻⁵³ when the Flory interaction parameter between DNA and the solution is known (Eqs. S29-S32).

Elastic Repulsion

The force that enforces a polymer chain to have a Gaussian conformation is known to contribute to the repulsive interaction potential, but only in the cases of extensively long DNA strands or single-stranded DNA at an elevated salt concentration.48,54 In the case of a rigid DNA duplex tethered to the particle's surface, when two particles come together to form a connection at a relatively short interparticle distance, a thermodynamic penalty involved in bending the DNA duplex due to its rigidity can play a role. When the elastic repulsion becomes greater than the strength of DNA hybridization interactions, it is favorable for the sticky ends to dehybridize. Therefore, the bending energy calculation will allow one to determine whether the conformational stresses imposed on DNA duplexes are enthalpically costly relative to the DNA hybridization interactions.

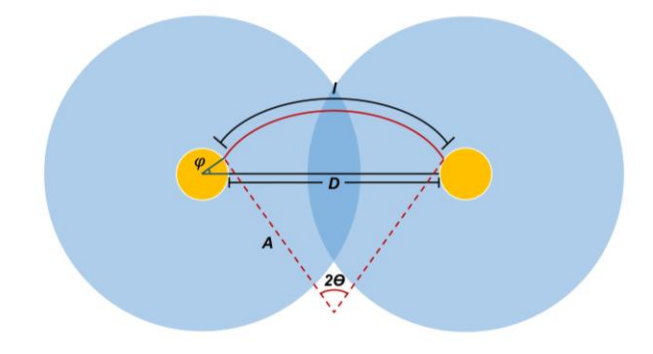


Figure 4. A geometric model showing different variables used to calculate the bending energy of DNA duplexes with a curvature *A*.

The stiffness of DNA duplex has been studied using the worm-like chain model, which is used to describe the behavior of semi-flexible polymer.^{21, 55-56} Therefore, in our the-

oretical model, the DNA duplex chain was assumed to behave like a cylindrical rod. Although the structure of DNA is more complex than a thin rod, the simple rod assumption has been used to describe the bending flexibility of DNA.²¹ By assuming that these chains will bend into an arc conformation upon compressive stress, the elastic energy was calculated.²¹ Indeed, this is a fair assumption because the flexor segment inserted between the sticky end and the duplexer region has been shown to serve as the focal point for bending.⁵⁷ Although it has been shown that the DNA bending energy is lower than the estimated energy from the classical elasticity model,²² we will use the bending energy predicted by Eq. 8 due to its simplicity:

$$E_b = \frac{Bl}{2A^2}$$
 Eq. 8

where E_b is the elastic energy of a single duplex chain (surface-to-surface connection), B is the bending elastic constant, l is the full length of a single duplex chain (equivalent to D in Figure 1b), and A is the arc radius (Figure 4). l can be calculated as $l = 2L_o - l_{sticky}$, where l_{sticky} is the length of a sticky end which consists of 7 bases (2.83 nm determined using Eq. S2). B can be calculated using this equation B/kT = P,55 where P is the persistence length of DNA duplex (50 nm). The elastic repulsion between a pair of PAEs $E_{Elastic}$ is calculated by taking the sum of all elastic repulsive potentials of DNA chains within the overlap:

$$E_{Elastic} = \sum E_b$$
 Eq. 9

The assumption underlying this calculation is that all DNA chains in the overlap are hybridized. Because the surface to which the DNA chains are tethered is curved, E_b for each DNA chain must be calculated by taking account of surface curvature (Eqs. S₃₃-S₃₈). This equation can be generalized to a set of two different sized PAEs (Eqs. S₃₉-S₄₄).

Repulsion from Entropic Effects due to Counterions

Due to its highly charged phosphate backbone, DNA is surrounded by mobile counterions to neutralize charge in aqueous media. It is well-understood that counterions condense onto polyelectrolytes until the charge density is reduced below the critical value, a phenomenon known as a Manning condensation.⁵⁸ As the DNA shells overlap, the volume in which the counterions can occupy decreases, and it results in an unfavorable decrease in entropy of the counterions. It has been shown that a relatively weak repulsion between star-shaped polyelectrolytes stems from the entropic effects due to the counterions that are trapped within the star's corona.23, 26 This concept has been extended to spherical brushes with a hard core.25 An analytical expression for the entropic repulsion when the interparticle distance is equal to d has been derived in previous literature (Eq. S₄₅).^{25, 59} Solving this equation demonstrates that the repulsive potential from entropic effects due to counterions, $E_{Entropy}$, is dependent on the number of counterions that are trapped within the overlap, n_{trap} . n_{trap}

is equivalent to the number of bases on a DNA chain because each base has one negative charge on the backbone:

$$n_{trap} = f_{trap} n_{base} \sigma$$
 Eq. 10

where f_{trap} is the fraction of unbounded counterions trapped in the overlap, which was assumed to be about 10%,⁵⁹ and n_{base} is the total number of DNA bases for each duplex chain. The volume that the trapped counterions can occupy is limited by the volume occupied by the DNA chains.

Potential Energy Calculation for PAE Superlattices

Based on the calculations using Eqs. 9 and 10, the contributions from both the DNA bending and the entropic effects of the trapped counterions have minimal effects on the overall interaction energy (Figure 5). The calculation of the elastic energy potential reveals that the bending energy increases when the gap distance becomes significantly smaller (Figure 5). However, the relative contribution of the elastic repulsion is negligible when compared with $E_{Attractive}$ and $E_{Excluded\ Volume}$. Likewise, $E_{Entropy}$ is small relative to the total pair potential, which coincides with the previous studies. ^{25, 45, 59}

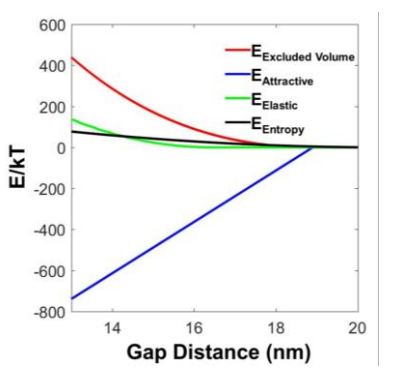


Figure 5. A comparison between $E_{Attractive}$, $E_{Excluded\ Volume}$, $E_{Elastic}$, and $E_{Entropy}$ calculated for 500 mM NaCl with constant L_o .

The pair potential energy E_{total} is the sum of $E_{Attractive}$ and $E_{Excluded\ Volume}$ (Figure 6a, Eq. S46). As discussed earlier, the comparison between the hybridization and the depletion based systems reveals that the repulsion is responsible for the observed power law behavior, meaning that the solution ionic strength has a relatively small effect on the attractive force. At 50 mM NaCl, the free energy at its minima lies at about -150 kT, indicating that the interaction is relatively weak. The free energy decreases to -350 kT at 500 mM NaCl, illustrating that the lattice has a greater stability at higher salt concentration. To validate our hypothesis about the role of repulsion in the superlattices, we plotted the distance at which the potential reaches its minima and compared this theory-derived curve with the experimentally determined curve shown in Figure 1a (Figure 6b). The simulations were performed with both constant and varying L_o as a function of salt concentration. The monotonically decaying trend is reproduced for both fixed and variable L_o (Figure 6b). However, a noticeable deviation in gap

distance at a low salt concentration regime between the experimental and the fixed L_o plots indicates that L_o varies with salt concentration (Figure 6b). Therefore, a good fit with experimental result can be obtained when L_o is varied as a function of salt concentration. This indicates that the expansion of DNA shell at lower salt concentration should be taken into consideration to build an accurate model for PAE interactions.

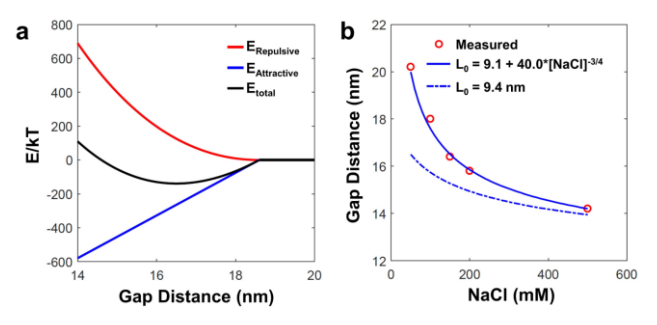


Figure 6. a) The theoretical interaction pair potential calculated for 500 mM NaCl condition with L_o varying as a function of [I]^{-3/4}. $E_{Repulsive}$ represents $E_{Excluded\ Volume}$ because it is the dominant repulsive potential based on Figure 5. b) The gap distances at its potential minima are plotted for various NaCl concentrations with fixed L_o (dashed blue line) and variable L_o (solid blue line), and were compared with the experimental data (hollow circle).

According to the classical polymer brush theory, L_0 of the grafted polyelectrolytes varies with salt concentration, where L_0 exhibits a relatively weak power law [I]^{-1/3}.²³ For our system, the best fit is observed with a stronger power law of [I]^{-3/4}, meaning the brush stretches to a greater degree with decreasing salt concentration (Figures 6b and S10). It is likely that the negative charge and the flexibility of the spacer and flexor segments allow the DNA to exhibit such strong salt-dependent behavior. The characteristic scaling exponent of -3/4 observed for our system is similar to the Alexander scaling behavior of the neutral brush thickness. 60 In both scaling laws, L_0 varies from about 11.2 nm at 50 mM NaCl to about 9.5 nm at 500 mM, roughly a 1.7 nm difference in L_o . In these calculations, DNA chains are assumed as continuum rods. However, the DNA used for this study contains both flexible single-stranded and rigid duplexed segments in different regions. Therefore, the scaling behavior observed for L_0 may not represent the behavior of DNA in its entirety. Assuming that the major length change comes from the flexible segments of the DNA chain (e.g. spacer and flexor segments, thus 2 nm at 500 mM for each chain, Eq. S2), we can estimate the possible length change for each scaling laws. According to the Pincus's scaling law, the flexible region extends up to 2 nm \cdot (50 mM/500 mM)^{-1/3} = 4.3 nm at 50 mM NaCl, thus the length change of 2.3 nm. When the Alexander's scaling law is applied, the flexible region lengthens to $2 \text{ nm} \cdot (50 \text{ m})$ $mM/500 \ mM)^{-3/4} = 11.2 \ nm$, which is unlikely because the difference is greater than the change in total DNA chain length. Nevertheless, the observed power law behavior of -

1/2 for D is different from the one observed for L_o . This further supports that the variation in DNA shell thickness is not the only factor that affects the salt-dependent repulsive interactions in PAE assembly (Eq. S47).

Using this model, we can calculate the lattice energy of PAE superlattices by considering both attractive and repulsive interactions of all interacting particles in each unit cell (Eq. S48). The major difference between the old model and this model is that this model allows one to account for pair interaction potentials between both complementary (both attraction and repulsion between unlike-particles, e.g. A-B pairs) and non-complementary (repulsion between likeparticles, e.g. A-A and B-B pairs) particles. For particles that have a gap distance farther than the sum of hydrodynamic radii of neighbor particles (e.g. there is no overlap), we assumed that there is no interaction. Therefore, in our bcc system, for example, the distance between like-particles was far enough such that the A-B pair interaction was sufficient to explain the overall lattice stability. However, in most cases, one must consider the pair potentials of all interacting particles to accurately portray the overall lattice energy. As a proof-of-concept, we show that the most stable c/a ratio for the AlB₂ structure is 0.91 for the given parameters, which coincides relatively well with the previously observed c/a ratio o.835 (Figure S11, Table S2). Additionally, the theoretically calculated interparticle distance of the AlB₂ lattice of 36.6 nm matches well with the experimentally determined value, 36.0 nm.5

Conclusion

In conclusion, this work shows that the dominant repulsion that counterbalances the DNA hybridization attraction is the excluded volume (steric) repulsion between DNA duplexes in PAE assembly. By employing two different attractive interactions, Watson-Crick base paring and depletion force, to assemble PAEs into well-defined structures, we observed a similar power law relationship between the gap distance and the salt concentration, confirming that the repulsion is responsible for the observed power law behavior. Three different types of repulsion were evaluated in this study: the excluded volume repulsion, elastic repulsion, and the repulsion from entropy due to counterions. We find that the steric repulsion, which varies as a function of L_0 and R_{DNA} , is the most important factor when calculating the pair potential of PAE superlattices. Finally, we developed a theoretical model that matches well with the experimentally observed power law behavior. These results highlight that repulsive forces play an important role in the crystallization behavior of PAEs and must be taken into account to fully understand and predict the assembly process and the energetics underlying

ASSOCIATED CONTENT

Supporting Information. [Oligonucleotide sequences, methods, step-by-step equation derivations, additional texts, figures, and tables]. This material is available free of charge via the Internet at http://pubs.acs.org.

AUTHOR INFORMATION

Corresponding Author

*Address correspondence to blee@aps.anl.gov and chadnano@northwestern.edu.

Author Contributions

The manuscript was written through contributions of all authors. All authors have given approval to the final version of the manuscript. ‡These authors contributed equally.

Notes

The authors declare no competing financial interest.

ACKNOWLEDGMENTS

This research used resources of the Advanced Photon Source, a U.S. Department of Energy (DOE) Office of Science User Facility operated for the DOE Office of Science by Argonne National Laboratory under Contract #DE-ACo2-o6CH11357. This work was also supported as part of the Center for Bio-Inspired Energy Science, an Energy Frontier Research Center funded by the U.S. Department of Energy, Office of Science, Basic Energy Sciences under Award #DE-SCoooo989. S.E.S. acknowledges partial support from the Center of Computation and Theory of Soft Materials at Northwestern University.

ABBREVIATIONS

PAE, DNA-modified particles; D, surface-to-surface distance between two nearest neighbor PAEs; I, salt concentration in mM; R, radius of a PAE; ρ_{DNA} , area fraction occupied by DNA duplexes; σ , number of DNA duplexes on a PAE; f_s , area fraction of the overlap between two PAEs; eh, hybridization energy of a sticky end; EAttractive, total hybridization energy between two PAEs; $E_{Repulsive}$, repulsive interaction potential energy; E_{Ex-} cluded Volume, excluded volume repulsive potential energy; E_{Elastic}, elastic potential energy; E_{Entropy}, repulsive potential energy from entropic effects due to counterions; R_{DNA}, effective crosssectional radius of a DNA duplex; r, radial distance from the center of PAE; κ^{-1} , the Debye length; R_0 , cross-sectional radius of a DNA duplex; V_{DNA}, volume occupied by DNA duplexes within the overlap; d, interparticle distance (center-to-center distance between two nearest neighbor PAEs); Π, osmotic pressure; V_o, total volume of the overlap; v, excluded volume of a monomer; c, concentration of monomers within the overlap; l_b , rise per base; ρ_0 , critical volume fraction of DNA duplex; r_o, radius of the critical volume fraction of DNA duplex (distance where interpenetration is prohibited); R_C, radius of gold core.

REFERENCES

- (1) Price, S. L. Chem. Soc. Rev. 2014, 43, 2098-2111.
- (2) Pauling, L. J. Am. Chem. Soc. 1929, 51, 1010-1026.
- (3) Woodley, S. M.; Catlow, R. Nat. Mater. 2008, 7, 937-946.
- (4) Macfarlane, R. J.; Jones, M. R.; Senesi, A. J.; Young, K. L.; Lee, B.; Wu, J.; Mirkin, C. A. *Angew. Chem.* **2010**, *122*, 4693-4696.
- (5) Macfarlane, R. J.; Lee, B.; Jones, M. R.; Harris, N.; Schatz, G. C.; Mirkin, C. A. *Science* **2011**, 334, 204-208.
- (6) Zhang, C.; Macfarlane, R. J.; Young, K. L.; Choi, C. H. J.; Hao, L.; Auyeung, E.; Liu, G.; Zhou, X.; Mirkin, C. A. *Nat. Mater.* **2013**, *12*, 741-746.

- (7) Zhang, Y.; Lu, F.; Yager, K. G.; van der Lelie, D.; Gang, O. *Nat. Nanotechnol.* 2013, 8, 865-872.
- (8) O'Brien, M. N.; Jones, M. R.; Lee, B.; Mirkin, C. A. *Nat. Mater.* **2015**, *14*, 833-839.
- (9) Seo, S. E.; Wang, M. X.; Shade, C. M.; Rouge, J. L.; Brown, K. A.; Mirkin, C. A. ACS Nano 2015, 10, 1771-1779.
- (10) Macfarlane, R. J.; Jones, M. R.; Lee, B.; Auyeung, E.; Mirkin, C. A. *Science* **2013**, *341*, 1222-1225.
- (11) Jones, M. R.; Macfarlane, R. J.; Lee, B.; Zhang, J.; Young, K. L.; Senesi, A. J.; Mirkin, C. A. Nat. Mater. 2010, 9, 913-917.
- (12) Park, S. Y.; Lytton-Jean, A. K.; Lee, B.; Weigand, S.; Schatz, G. C.; Mirkin, C. A. *Nature* **2008**, 451, 553-556.
- (13) Auyeung, E.; Cutler, J. I.; Macfarlane, R. J.; Jones, M. R.; Wu, J.; Liu, G.; Zhang, K.; Osberg, K. D.; Mirkin, C. A. *Nat. Nanotechnol.* **2012**, *7*, 24-28.
- (14) Thaner, R. V.; Eryazici, I.; Macfarlane, R. J.; Brown, K. A.; Lee, B.; Nguyen, S. T.; Mirkin, C. A. *J. Am. Chem. Soc.* **2016**, *1*38, 6119-6122.
- (15) Thaner, R. V.; Kim, Y.; Li, T. I. N. G.; Macfarlane, R. J.; Nguyen, S. T.; Olvera de la Cruz, M.; Mirkin, C. A. *Nano Lett.* **2015**, *1*5, 5545-5551.
- (16) Vo, T.; Venkatasubramanian, V.; Kumar, S.; Srinivasan, B.; Pal, S.; Zhang, Y.; Gang, O. *Proc. Natl. Acad. Sci.* **2015**, *112*, 4982-4987.
- (17) Jones, M. R.; Macfarlane, R. J.; Prigodich, A. E.; Patel, P. C.; Mirkin, C. A. *J. Am. Chem. Soc.* **2011**, *133*, 18865-18869.
- (18) Maye, M. M.; Nykypanchuk, D.; van der Lelie, D.; Gang, O. *Small* **2007**, 3, 1678-1682.
- (19) Lee, S.; Leighton, C.; Bates, F. S. *Proc. Natl. Acad. Sci.* **2014**, *111*, 17723-17731.
- (20) Baumann, C. G.; Smith, S. B.; Bloomfield, V. A.; Bustamante, C. Proc. Natl. Acad. Sci. 1997, 94, 6185-6190.
 - (21) Marko, J. F.; Cocco, S. Physics World 2003, 16, 37.
- (22) Wiggins, P. A.; Van Der Heijden, T.; Moreno-Herrero, F.; Spakowitz, A.; Phillips, R.; Widom, J.; Dekker, C.; Nelson, P. C. *Nat. Nanotechnol.* 2006, *1*, 137-141.
 - (23) Pincus, P. Macromolecules 1991, 24, 2912-2919.
- (24) Dobrynin, A. V.; Colby, R. H.; Rubinstein, M. *Macromolecules* **1995**, *28*, 1859-1871.
- (25) Jusufi, A.; Likos, C.; Ballauff, M. Colloid. Polym. Sci. 2004, 282, 910-917.
- (26) Jusufi, A.; Likos, C.; Löwen, H. *J. Chem. Phys.* **2002**, *116*, 11011-11027.
- (27) Ross, M. B.; Ku, J. C.; Vaccarezza, V. M.; Schatz, G. C.; Mirkin, C. A. *Nat. Nanotechnol.* **2015**, *10*, 453-458.
- (28) Sun, S.; Murray, C.; Weller, D.; Folks, L.; Moser, A. *Science* **2000**, 287, 1989-1992.
- (29) Mason, J. A.; Laramy, C. R.; Lai, C.-T.; O'Brien, M. N.; Lin, Q.-Y.; Dravid, V. P.; Schatz, G. C.; Mirkin, C. A. *J. Am. Chem. Soc.* **2016**, *1*38, 8722-8725.
 - (30) Li, T.; Senesi, A. J.; Lee, B. Chem. Rev. 2016, 116, 11128-11180.
- (31) Kewalramani, S.; Zwanikken, J. W.; Macfarlane, R. J.; Leung, C.-Y.; Olvera de la Cruz, M.; Mirkin, C. A.; Bedzyk, M. J. ACS Nano **2013**, *7*, 11301-11309.
- (32) Senesi, A. J.; Eichelsdoerfer, D. J.; Brown, K. A.; Lee, B.; Auyeung, E.; Choi, C. H. J.; Macfarlane, R. J.; Young, K. L.; Mirkin, C. A. *Adv. Mater.* **2014**, *26*, 7235-7240.
- (33) Podgornik, R.; Hansen, P. L.; Parsegian, V. A. *J. Chem. Phys.* **2000**, *11*3, 9343-9350.
- (34) Wenner, J. R.; Williams, M. C.; Rouzina, I.; Bloomfield, V. A. *Biophys. J.* **2002**, *82*, 3160-3169.
- (35) Hagerman, P. J. Annu. Rev. Biophys. Biomol. Struct. 1988, 17, 265-286.
 - (36) Lei, Q.-l.; Ren, C.-l.; Su, X.-h.; Ma, Y.-q. Sci. Rep. 2015, 5.

- (37) Mirkin, C. A.; Letsinger, R. L.; Mucic, R. C.; Storhoff, J. J. *Nature* **1996**, 607-9.
 - (38) Tan, Z.-J.; Chen, S.-J. J. Chem. Phys. 2005, 122, 044903.
- (39) Qiao, W.; Chiang, H.-C.; Xie, H.; Levicky, R. *Chem. Commun.* **2015**, *51*, 17245-17248.
- (40) Li, T.; Zan, X.; Winans, R. E.; Wang, Q.; Lee, B. Angew. Chem., Int. Ed. 2013, 52, 6638-6642.
- (41) Asakura, S.; Oosawa, F. J. Polym. Sci., Part A 1958, 33, 183-192.
- (42) Young, K. L.; Jones, M. R.; Zhang, J.; Macfarlane, R. J.; Esquivel-Sirvent, R.; Nap, R. J.; Wu, J.; Schatz, G. C.; Lee, B.; Mirkin, C. A. *Proc. Natl. Acad. Sci.* 2012, 109, 2240-2245.
- (43) Young, K. L.; Personick, M. L.; Engel, M.; Damasceno, P. F.; Barnaby, S. N.; Bleher, R.; Li, T.; Glotzer, S. C.; Lee, B.; Mirkin, C. A. *Angew. Chem., Int. Ed.* **2013**, *52*, 13980-13984.
- (44) Naji, A.; Seidel, C.; Netz, R. R., Theoretical Approaches to Neutral and Charged Polymer Brushes. In *Surface-Initiated Polymerization II*, Jordan, R., Ed. Springer Berlin Heidelberg: Berlin, Heidelberg, **2006**, 149-183.
 - (45) Ballauff, M. Prog. Polym. Sci. 2007, 32, 1135-1151.
- (46) Jin, R.; Wu, G.; Li, Z.; Mirkin, C. A.; Schatz, G. C. *J. Am. Chem. Soc.* **2003**, *125*, 1643-1654.
- (47) Konieczny, M.; Likos, C. N. *J. Chem. Phys.* **2006**, *124*, 214904.

- (48) Tkachenko, A. V. Phys. Rev. Lett. 2002, 89, 148303.
- (49) Milner, S. T.; Witten, T. A.; Cates, M. E. *Macromolecules* 1988, 21, 2610-2619.
- (50) Tokuda, J. M.; Pabit, S. A.; Pollack, L. *Biophys. Rev.* **2016**, *8*, 139-149.
 - (51) Sinden, R. R., DNA Structure and Function. Elsevier: 2012.
 - (52) Napper, D. H. J. Colloid Interface Sci. 1977, 58, 390-407.
- (53) Flory, P. J., *Principles of Polymer Chemistry*. Cornell University Press: 1953.
- (54) Valignat, M.-P.; Theodoly, O.; Crocker, J. C.; Russel, W. B.; Chaikin, P. M. *Proc. Natl. Acad. Sci.* **2005**, *102*, 4225-4229.
- (55) Baumann, C. G.; Smith, S. B.; Bloomfield, V. A.; Bustamante, C. *Proc. Natl. Acad. Sci.* **1997**, *94*, 6185-6190.
- (56) Bustamante, C.; Marko, J. F.; Siggia, E. D.; Smith, S. Science-New York Then Washington- 1994, 1599-1599.
- (57) Lee, O.-S.; Cho, V. Y.; Schatz, G. C. *J. Phys. Chem. B* **2012**, *116*, 7000-7005.
 - (58) Manning, G. S. J. Chem. Phys. 1969, 51, 924-933.
- (59) Kegler, K.; Konieczny, M.; Dominguez-Espinosa, G.; Gutsche, C.; Salomo, M.; Kremer, F.; Likos, C. N. *Phys. Rev. Lett.* **2008**, *100*, 118302.
 - (60) Alexander, S. J. Phys. 1977, 38, 983-987.

For Table of Contents Only

